Quality of the restricted variation after projection method with angular momentum projection

Tomás R. Rodríguez,* J. L. Egido,† and L. M. Robledo‡

Departamento de Física Teórica C-XI, Facultad de Ciencias, Universidad Autónoma de Madrid, 28049 Madrid, Spain

R. Rodríguez-Guzmán§

Institut für Theoretische Physik der Universität Tübingen, D-72076 Tübingen, Germany

Recently, the restricted angular momentum variation after projection method, using the quadrupole degree of freedom as a variational coordinate in conjunction with effective interactions of the Skyrme or Gogny type, has been used very successfully to study a variety of phenomena concerning the quadrupole degree of freedom. In this paper, we study the quality of such an approach by considering additional degrees of freedom as variational coordinates: the hexadecapole moment and the fluctuations on the quadrupole moment, particle number, and angular momentum operators. The study has been performed with the Gogny interaction ($D1S$ parametrization) for the nuclei ^{32}Mg and ^{34}Mg. The results of the angular momentum projection and the subsequent generator coordinate calculations show that the extra degrees of freedom considered are irrelevant for the description of the lowest lying states for each angular momentum.

I. INTRODUCTION

Currently, mean field calculations like the ones based on the Hartree-Fock-Bogoliubov (HFB) method are routinely carried out (see Ref. [1] for a recent review) with effective phenomenological interactions like Skyrme or Gogny in order to study nuclear bulk properties in a systematic way. These studies have opened up the possibility of confronting theory (both the method and the interactions) with experiment all over the nuclide chart. The conclusions reached in such studies confirm the validity of both the mean field concept and the associated spontaneous symmetry breaking mechanism leading to nuclear super-fluidity, shape deformations, etc. (see Ref. [2] for a recent example). However, there are several examples, scattered all over the nuclide chart, indicating that the correlations associated with the restoration of symmetries broken at the mean field level can substantially modify the mean field picture. Perhaps the best known of these examples is the ground state of ^{32}Mg, which is predicted to be spherical at the mean field level with most of the reasonable interactions available in the market [3–6] but always turns out to be quadrupole deformed when the correlation energy associated with the restoration of the broken rotational symmetry is considered [7,8]. Experimentally, this nucleus is assumed to be deformed, in spite of being semimagic ($N = 20$), because of the low excitation energy of the first 2^+ state and also because of the ratio $E(4^+)/E(2^+) = 2.6$, which is consistent with the expectations for a rotational (and therefore deformed) state [9,10]. Measurements of the $B(E2, 0_1^+ \rightarrow 2_1^+)$ transition probabilities also strongly support the interpretation in terms of a deformed intrinsic state [11–14].

To restore the rotational symmetry broken by the intrinsic state, the angular momentum projection (AMP) technique is used (see [15,16] for a detailed account of the theory and [1,17,18] for additional considerations in the case of density dependent interactions). In the AMP method, a symmetry breaking intrinsic state is projected onto good angular momentum J by taking linear combinations of properly weighted wave functions obtained by rotating the intrinsic state. There are two ways [15] to consider the effect of symmetry restoration on the energy. The easiest one, called projection after variation (PAV), starts with the mean field ground state solution, which is projected afterward onto the proper quantum numbers, and the resulting wave functions are used to compute the projected energies. By definition, this procedure excludes the possibility of having intrinsic wave functions with a projected energy lower than the one obtained from the intrinsic ground state; that is, the intrinsic ground state minimum is assumed to be sitting on the bottom of a deep enough well. However, it is known that this is not the case in the nucleus ^{32}Mg, for example, where the spherical mean field absolute minimum is not deep enough, and therefore there exist other deformed mean field solutions that lead to a projected energy lower than the one of the spherical intrinsic state [7,8]. To overcome this deficiency, the variation after projection (VAP) method was introduced. In this method, the optimum intrinsic states are searched for by minimizing the projected energy for each value of J instead of the HFB one [15]. Unfortunately, this is a rather sophisticated and computationally demanding procedure, and therefore it has only been implemented in small configuration spaces so far (see Ref. [19] for a recent theoretical account). A simplifying alternative is to perform a VAP calculation but over a reduced (a physically inspired) subset of the whole variational space available for the intrinsic configurations. For instance, in the ^{32}Mg case [18], a reduced set of intrinsic mean field configurations was determined by constraining the axial quadrupole operator, and the optimum intrinsic configurations were chosen by requiring

*Email address: Tomas.Rodriguez@uam.es
†Email address: J.Luis.Egido@uam.es
‡Email address: Luis.Robledo@uam.es
§Email address: rayner@tphys.physik.uni-tuebingen.de

the projected energy for each value of J to yield an absolute minimum. In this way, a deformed intrinsic state was predicted for the 0^+ ground state in opposition to the spherical one predicted by the mean field. Obviously, the success of such a restricted VAP procedure is linked to the adequacy of the reduced variational space for the physics involved. In the case of AMP, it seems rather natural to assume that the axial quadrupole degree of freedom is going to play an important role as this is the lowest order multipole moment linked to spatial deformation. This is the reason why most of the calculations performed to date with effective forces and along the lines described previously have used this collective variable to generate the reduced configuration space. However, other degrees of freedom such as (a) higher order axial multipole moments, (b) fluctuations on the multipole moments, (c) fluctuations on the angular momentum operators, (d) fluctuations on particle number (pairing correlations), (e) reflection asymmetric multipole moments (octupole shapes), (f) triaxial moments, and (g) time reversal breaking degrees of freedom (such as the ones induced by the cranking approximation) could be needed for a more accurate description of nuclear dynamics, and therefore they deserve further investigation.

In this paper, we have addressed the study of the role of some of the degrees of freedom mentioned above by performing calculations with the Gogny interaction [20] ($D1S$ parametrization [21]) for the ^{32}Mg and ^{34}Mg nuclei. For computational reasons, the calculations have been restricted to axial and reflection symmetric intrinsic configurations (see Ref. [18] for further details), and therefore we have been unable to study the effect of reflection asymmetry, triaxiality, and time reversal breaking configurations. Reflection asymmetry is supposed not to play a relevant role in the magnesium isotopes, making its omission somehow justified. However, the other two neglected degrees of freedom (triaxiality and time reversal breaking) certainly play an important role for $J \neq 0$ states, restricting our conclusions mainly to the $J = 0^+$ states (including the ground state). Although our results indicate that the extra degrees of freedom considered (the hexadecapole moment $\hat{Q}_{40}$ and the fluctuations in the quadrupole moment $(\Delta \hat{Q}_{20})^2$, angular momentum $\Delta \hat{J}_x^2$, and particle number $(\Delta \hat{N})^2$) do not substantially modify the predictions already obtained with the axial quadrupole moment $\hat{Q}_{20}$ alone, we have also carried out configuration mixing calculations in the spirit of the generator coordinate method (GCM) and using the axial quadrupole degree of freedom as a generating coordinate in order to make sure that the dynamical aspects are not altered by the tiny changes induced by considering the additional operators. A preliminary account of the present work but considering only the hexadecapole and particle number fluctuations and without considering the GCM results has already been published [22].

The paper is organized as follows. In Sec. II, the method used is discussed in detail, and the selection of the additional degrees of freedom is discussed and justified. In Sec. III, the results obtained are analyzed, and finally in Sec. IV, some conclusion are drawn.

II. THEORETICAL FRAMEWORK: RESTRICTED PROJECTION BEFORE VARIATION WITH CONSTRAINED HFB INTRINSIC STATES

Our starting point in the generation of a restricted variational space is a set of constrained Hartree-Fock-Bogoliubov (CHFB) calculations with two constraints at a time (apart from the ones on proton and neutron particle numbers that are always included in the HFB method):

$$\langle \phi(q,s)|\hat{Q}_{20}|\phi(q,s)\rangle = q, \qquad \langle \phi(q,s)|\hat{S}|\phi(q,s)\rangle = s. \tag{1}$$

The first constraint refers to the axial quadrupole moment q, which is restricted to its $K = 0$ component as a consequence of our restriction to axially symmetric and parity conserving configurations. In the second constraint, the operator $\hat{S}$ stands for any of the additional degrees of freedom considered. The set of wave functions $|\phi(q,s)\rangle$ is determined by minimizing the HFB energy $E(q,s) = \langle \phi(q,s)|\hat{H}|\phi(q,s)\rangle$ subject to the constraints of Eq. (1). The constrained minimization process is equivalent to the solution of the HFB equation $\delta\langle \phi(q,s)|\hat{H}'|\phi(q,s)\rangle = 0$ where $\hat{H}' = \hat{H} - \lambda_q(\hat{Q}_{20} - q) - \lambda_s(\hat{S} - s)$, and the Lagrange multipliers λ_q and λ_s are determined in the usual way by requiring the gradient of the constraint to be orthogonal to the gradient of $\langle \phi(q,s)|\hat{H}'|\phi(q,s)\rangle$. The CHFB equation is solved using the gradient method [23] as it has the advantage of being very well suited for the handling of many constraints at the same time. Another merit of the gradient method is that it is also very well suited for the handling of two body operators as constraints. The HFB equation is solved with the Gogny interaction [20] ($D1S$ parametrization [21]). As is customary in these kinds of calculations, we have fully included the two body kinetic energy correction (to correct for the center of mass motion problem) but neglected the Coulomb exchange and pairing fields. The range of q values considered starts at -2 b and goes up to 2 b in steps of 0.05 b and is well suited for both the ^{32}Mg and ^{34}Mg nuclei. For the quantity s, we consider a range of values depending on q and centered around the self-consistent value $s_{SC}(q)$, which is determined by releasing the constraint on that quantity and keeping only the constraint on the quadrupole moment.

After the set of wave functions $|\phi(q,s)\rangle$ is determined, we compute the angular momentum projected (AMP) energies for each value of $J = 0, 2, 4, \ldots$, as

$$E^J(q,s) = \frac{\langle \phi(q,s)|\hat{H}\hat{P}_{00}^J|\phi(q,s)\rangle}{\langle \phi(q,s)|\hat{P}_{00}^J|\phi(q,s)\rangle}, \tag{2}$$

where $\hat{P}_{00}^J$ is the angular momentum projection operator for axially symmetric intrinsic states. These projected energies define a two-dimensional potential energy surface (PES) as a function of (q,s) whose minimum provides the solution of this restricted VAP procedure.

Concerning the set of additional constraining operators $\hat{S}$ considered, we have included the next even order multipole moment, i.e., the hexadecapole moment $\hat{Q}_{40}$, in order to better explore the variety of (reflection symmetric) nuclear shapes. Next we have considered the quadrupole fluctuations given by

the two body operator $(\Delta\hat{Q}_{20})^2$, where $\Delta\hat{Q}_{20} = \hat{Q}_{20} - \langle\hat{Q}_{20}\rangle$. Taking for granted that the rotational energy correction (the energy gain with respect to the mean field) is proportional to the fluctuations in the angular momentum operators, we have also considered as a constraining operator the fluctuation in $\hat{J}_x$; namely, we have used the two body operator $(\Delta\hat{J}_x)^2$, where $\Delta\hat{J}_x = \hat{J}_x - \langle\hat{J}_x\rangle = \hat{J}_x$ (the last equality is due to the fact that we consider axially symmetric wave functions in even-even nuclei). Finally, and taking into account the predominant role that the pairing degree of freedom plays in the determination of moments of inertia (the other quantity entering the rotational energy correction), we have also performed calculations constraining the fluctuations of the particle number $(\Delta\hat{N})^2$ as a device to modulate pairing correlations or the smearing out of the Fermi surface.

The topological structure of the AMP potential energy surface in ^{32}Mg as a function of q alone (flat minima separated by rather small barriers) suggested [18] that configuration mixing in the spirit of the generator coordinate method (GCM) using the axial quadrupole moment as a generating coordinate would be of paramount importance in the description of this particular system. As we see in the next section, the same kind of arguments applied to the present calculations call for a GCM calculation including both the q and s degrees of freedom. However, this is a highly demanding task (it would increase the computational burden by two orders of magnitude), and therefore we have restricted ourselves to performing GCM calculations using the quadrupole moment q as a generating coordinate, and the value of s determined by the minimum of the projected energy $E^J(q, s)$ for each value of q and J. In other words, we use as the GCM wave functions the ansatz

$$\left|\Psi_\sigma^J\right\rangle = \int dq\, f_\sigma^J(q)\hat{P}^J|\phi(q, s^J(q))\rangle,$$

where the set of functions $s^J(q)$ is determined by requiring $E^J(q, s)$ to be a minimum for fixed values of q.

III. RESULTS

In this section we show the results for ^{32}Mg and ^{34}Mg using the theoretical tools described in the previous section. For the convenience of the reader, we begin by briefly discussing the results obtained with the single constraint on the axial quadrupole moment q for ^{32}Mg. The energies of the q-constrained HFB calculation, as well as the ones corresponding to the AMP for $J = 0, 2$, and 4, are shown in Fig. 1. At the mean field level, the ^{32}Mg ground state has a spherical absolute minimum, as well as a shoulder around $q = 1$b. On the other hand, the projected energy for $J = 0$ exhibits both prolate and oblate minima located at 1.0 and -0.5 b, respectively. The ground state corresponds to the prolate shape. This example clearly shows how the plain PAV procedure provides incorrect results. In the strict PAV approach, one would first solve the self-consistent HFB equation and then perform AMP. In this case, since the self-consistent solution is spherical, one would obtain no energy gain at all. However, by looking at the reduced space of the quadrupole deformed axial shapes (in the spirit of the restricted VAP) we find deeper minima than
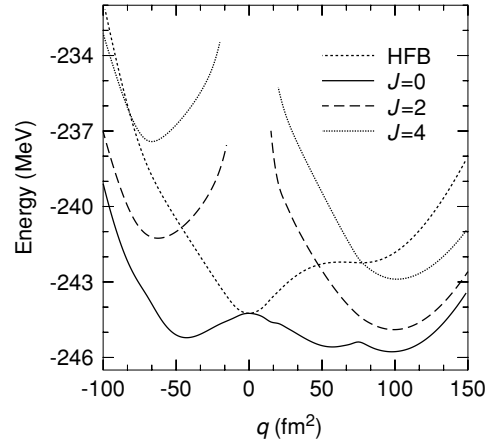
FIG. 1. Single-constraint HFB and angular momentum projected potential energy surfaces for ^{32}Mg as a function of the quadrupole moment $q = \langle\hat{Q}_{20}\rangle$.

the spherical one, and therefore a completely different physical picture emerges.

The next step is now to perform double constrained calculations as described in the previous section. In Fig. 2, we present a representative selection of the results obtained by plotting cuts of $E^J(q, s)$ for $q = -0.5$ and 1 b as a function of s for the different constraining operators $\hat{S}$ considered, namely, the hexadecapole moment $\hat{Q}_{40}$ (panels (a) and (b)), the fluctuation in the number of particles $(\Delta\hat{N})^2$ (panels (c) and (d)), the fluctuation in the quadrupole moment $(\Delta\hat{Q}_{20})^2$ (panels (e) and (f)), and finally the fluctuation in the angular momentum operator $(\Delta\hat{J}_x)^2$ (panels (g) and (h)). The bullets on each curve are placed at the corresponding minima, and the vertical lines pass through the minimum of the HFB energy curve, i.e., the value found without constraining $\hat{S}$. For a given value of J, the energy gain obtained by constraining the additional operator is given by the energy difference between the projected energy at the minimum (marked by the bullets) and the projected energy obtained at the intersection of the vertical line with the AMP energy curve. For $J = 0$, the projected energy minima remain rather close to the single constraint results for both the prolate and oblate examples shown in Fig. 2, and therefore the effect of the additional constraints is negligible. For $J = 2$, the situation changes: although the minima are the same as in the single constraint case for the prolate configuration, we observe noticeable differences in the oblate configuration considered. This can be understood by the fact that the prolate deformation (1 b) is larger than the oblate one (-0.5 b), and the HFB approach is better for larger deformations. It is also noticeable that the largest corrections are obtained for the $\langle\Delta\hat{N}^2\rangle$ and $\langle\Delta\hat{J}_x^2\rangle$ constraints. The same tendency as in the $J = 2$ case, but amplified, is obtained for $J = 4$. The numerical values for the energy gain for the operators and J values considered are given in Table I. The small energy corrections obtained for $J = 0$ indicate that the energy minimum obtained with only the constraint on $\hat{Q}_{20}$ provides a rather stable minimum, probably close to the true VAP one. We cannot say the same for higher J values and the oblate configurations.
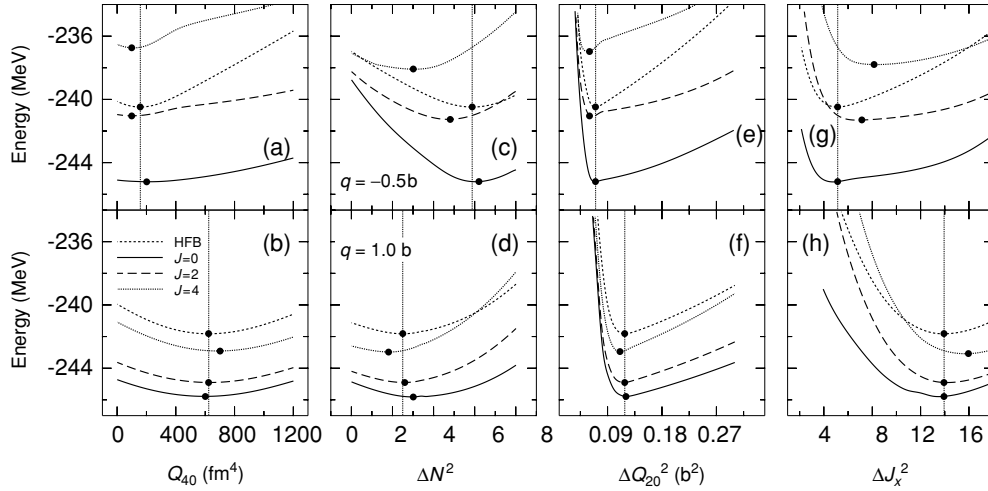
FIG. 2. The projected energies $E^J(q, s)$ as a function of s for the four additional constraining operators considered and the $q = \langle \hat{Q}_{20} \rangle$ values of 1 (lower panels) and -0.5 b (upper panels). The bullets mark the position of the minima. The dashed curves correspond to the HFB solutions. The vertical dotted lines mark the minima of the HFB curves. See text for further details.

In order to better understand the effect of the additional constraints on the results of Fig. 2, we have plotted in Fig. 3 the energy differences $E^J(q, s) - E_{\mathrm{HFB}}(q, s)$ for $J = 0$, 2, and 4 as a function of the constraining quantities s and the q values 1 and -0.5 b. In order to clarify the discussion of these results, it is convenient to introduce the "strong deformation limit" of the projected energies [15,17]

$$
E^J(q, s) \approx \langle \phi(q, s) | \hat{H} | \phi(q, s) \rangle
$$
$$
- \frac{\langle \phi(q, s) | \hat{\vec{J}}^2 | \phi(q, s) \rangle}{2 \mathcal{J}_Y(q, s)} + \hbar^2 \frac{J(J+1)}{2 \mathcal{J}_Y(q, s)}.
$$

The first term is simply the intrinsic energy; the second, called the "rotational energy correction" (REC), is the ratio between the fluctuations of the angular momentum operator and the Yoccoz moment of inertia $\mathcal{J}_Y$; and the third one is just the rotational band energy that follows the rigid rotor $J(J+1)$ energy rule. The rotational energy correction is the energy gain due to the additional correlations introduced by the projection procedure, and its evolution with s depends on the evolution of both the fluctuations on the angular momentum and the evolution of the Yoccoz moment of inertia. On the other hand, the rotational band energy only depends on the Yoccoz moment of inertia, and therefore its behavior with s can be rather different from that of the REC. Obviously, the

$J = 0$ energy difference depicted in Fig. 3 is nothing but the rotational energy correction. On the other hand, it is obvious that the other curves will remain parallel to the $J = 0$ one in the case in which the Yoccoz moment of inertia does not change with the constraining quantity s. When the moment of inertia increases with increasing values of the additional constraint, the lines will converge, whereas for a decreasing moment of inertia, the lines will diverge.

By looking at panels (a) and (b) of Fig. 3, we realize that the constraint on the hexadecapole moment do not change the Yoccoz moment of inertia in both cases, as the projected energy curves remain more or less parallel. The same happens for the rotational energy correction (REC) in the prolate cut. On the other hand, the REC increases with an increasing hexadecapole moment in the oblate cut. For the constraint on the particle number fluctuation (panels (c) and (d)), we observe how the projected energy curves diverge as $\langle \Delta \hat{N}^2 \rangle$ increases, implying the decrease of the Yoccoz moment of inertia. This is consistent with the general consensus (see, for instance, [15]) that moments of inertia decrease with increasing pairing correlations. The moment of inertia decreases faster in the oblate than in the prolate case. The REC slightly increases as a function of $\langle \Delta \hat{N}^2 \rangle$ in the prolate side, but the increase is a little more pronounced in the oblate one. This behavior, together with the behavior of the moment

TABLE I. Energy gains ΔE^J for angular momenta $J = 0$, 2, and 4 obtained for the quadrupole moment values $q = -0.5$ and 1 b by constraining the additional operators considered.

$\hat{S}$	q (b)	$\Delta E^{J=0}$ (keV)	$\Delta E^{J=2}$ (keV)	$\Delta E^{J=4}$ (keV)	q (b)	$\Delta E^{J=0}$ (keV)	$\Delta E^{J=2}$ (keV)	$\Delta E^{J=4}$ (keV)
$\hat{Q}_{40}$	-0.5	8.0	19.0	39.0	1.0	1.0	0.0	14.0
$(\Delta \hat{N})^2$	-0.5	6.0	250.0	1401.0	1.0	30.0	0.0	79.0
$(\Delta \hat{Q}_{20})^2$	-0.5	0.0	40.0	278.0	1.0	0.0	0.0	67.0
$(\Delta \hat{J}_x)^2$	-0.5	0.0	297.0	1103.0	1.0	0.0	0.0	192.0
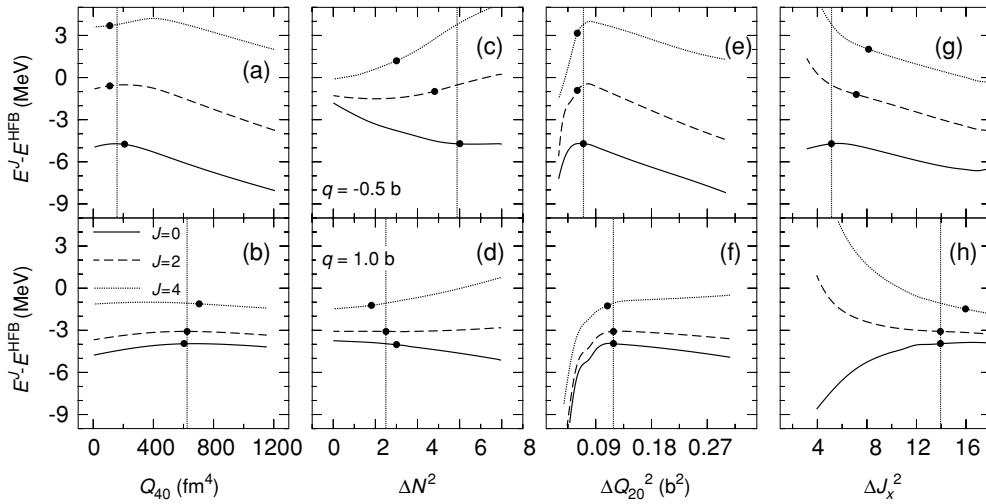
FIG. 3. The energy differences $E^J(q, s) - E_{HFB}(q, s)$ as a function of s for the four additional constraining operators considered for the $q = \langle \hat{Q}_{20} \rangle$ values of 1 b (lower panels) and -0.5 b (upper panels). The bullets mark the positions of the minima of the corresponding $E^J(q, s)$ curves, whereas the vertical dotted lines mark the positions of the HFB minima. See text for further details.

of inertia, implies that $\langle \Delta \hat{J}_x^2 \rangle$ decreases with increasing particle number fluctuations. For the constraint on the quadrupole moment fluctuation, we observe a pattern similar to that in the hexadecapole case. One noticeable difference is that in the prolate side, the moment of inertia slightly decreases with $\langle (\Delta \hat{Q}_{20})^2 \rangle$, whereas it slightly increases with increasing $\langle \hat{Q}_{40} \rangle$. A second difference is the violent increase in the REC energy observed when the quadrupole fluctuation is reduced with respect to the self-consistent minimum. For the angular momentum fluctuation constraint, the Yoccoz moment of inertia increases, with the increasing $\langle \Delta \hat{J}_x^2 \rangle$ being the increment more pronounced in the prolate than in the oblate side. This behavior is due to the fact that bigger values of $\langle \Delta \hat{J}_x^2 \rangle$ imply a stronger rotational symmetry violation and therefore bigger moments of inertia. As a consequence of the increase of the moment of inertia with $\langle \Delta \hat{J}_x^2 \rangle$, the REC decreases with increasing fluctuation in the prolate case, whereas it slightly increases in the oblate case.

In Fig. 4 we have plotted, for the nucleus ^{32}Mg, the projected energies for $J = 0$, 2, and 4 corresponding to the minima of the curves of Fig. 2 but for all values of the quadrupole moment q (solid line) along with the projected energies obtained for the self-consistent value of $\langle \hat{S} \rangle$ (dashed line) corresponding to the intrinsic energy. We observe that the solid and dashed lines are almost indistinguishable for $J = 0$, with the exception of the constraints on $\langle \Delta \hat{N}^2 \rangle$ and $\langle \Delta \hat{J}_x^2 \rangle$ and for q values around the kink at 75 fm^2. For $J = 2$, solid and dashed lines are again almost indistinguishable around the prolate minima but show small deviations for the oblate ones. For $J = 4$, appreciable differences are seen in the oblate side which is, however, not the absolute minimum for this value of the angular momentum. These results indicate that the extra degrees of freedom considered are of no relevance for the description of the lowest lying state for each angular momentum J. For higher lying states with $J = 2$ and 4 and sitting in the oblate minimum, the energies will certainly change and the effect of the additional degrees of freedom can be relevant. In Fig. 5 we

have plotted the same quantities as in Fig. 4 but for the nucleus ^{34}Mg. Behavior similar to that in the ^{32}Mg case is observed, and therefore the conclusions to be drawn are the same.

Although the projected energies are not much affected in the vicinity of the absolute minimum for each angular momentum considered as a consequence of the second constraint, it might well happen that the slight changes induced in the wave functions could modify the dynamical aspects of the problem, and for this reason we have performed GCM calculations for the nucleus ^{32}Mg along the lines described in Sec. III for each of the additional constraints and for $J = 0$, 2, and 4. By looking at the rather flat projected energy curves as a function of s depicted in Fig. 2, and also taking into account that their topologies change with angular momentum (see also the discussion of Fig. 3), one can easily see that a better approach would be to perform just a two-dimensional GCM calculation. Unfortunately, this task is still too time consuming (increasing the computational burden by two orders of magnitude), and therefore we have restricted ourselves to the less general procedure outlined in Sec. II. The results of the GCM calculations are summarized in Table II. As can be observed in Table II, the energy gains for the $J = 0$ ground states are tiny, and a maximum value of 93 keV is reached for the $\langle \Delta \hat{N}^2 \rangle$ constraint. Obviously, these small changes are of the order of magnitude of the uncertainties associated with the parameters of the interaction and/or issues related to the finite size of the basis and therefore can be safely overlooked. For $J = 2$, the changes are even smaller than for the $J = 0$ case, as expected from Fig. 4. As a consequence, the changes in the E_{2^+} excitation energies come mainly from the decrease of the $J = 0$ energies, and the biggest one, corresponding to the $\langle \Delta \hat{N}^2 \rangle$ additional constraint, amounts to an increase of 89 keV, which represents a small fraction (a 5% effect) of the absolute value and is also of the order of magnitude of other uncertainties that could eventually affect the E_{2^+} energies as discussed previously. The results obtained are in agreement with the general considerations
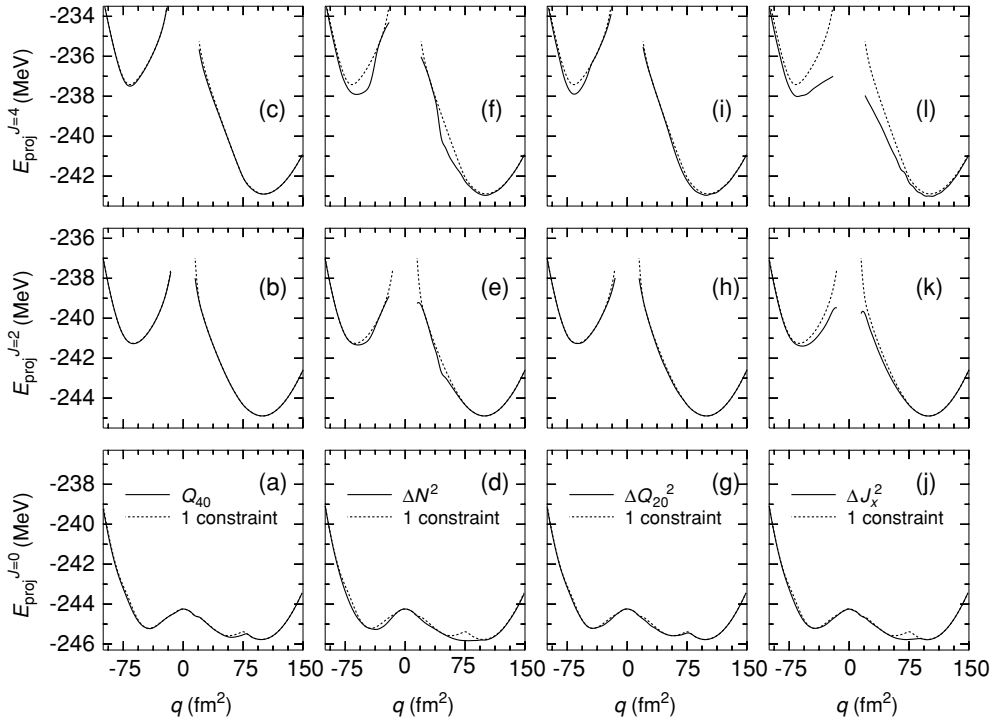
FIG. 4. A comparison of the projected energy curves $E^J(q,s)$ with s determined as the minimum of $E^J(q,s)$ for each value of $q = \langle \hat{Q}_{20} \rangle$ (solid line), and the same quantity but with s given by the HFB self-consistent value (dashed curves) for $J = 0$ (lower panels), 2 (middle panels), and 4 (upper panels) and the four additional constraints considered.

drawn from similar calculations [19]: whenever additional correlations are included, the 0^+ gets pushed down, and therefore excitation energies tend to increase. Unfortunately, this behavior is the opposite of that needed to improve the agreement with the experimental results [9,10]. As previously discussed [8], in order to decrease the E_{2^+} excitation energy,
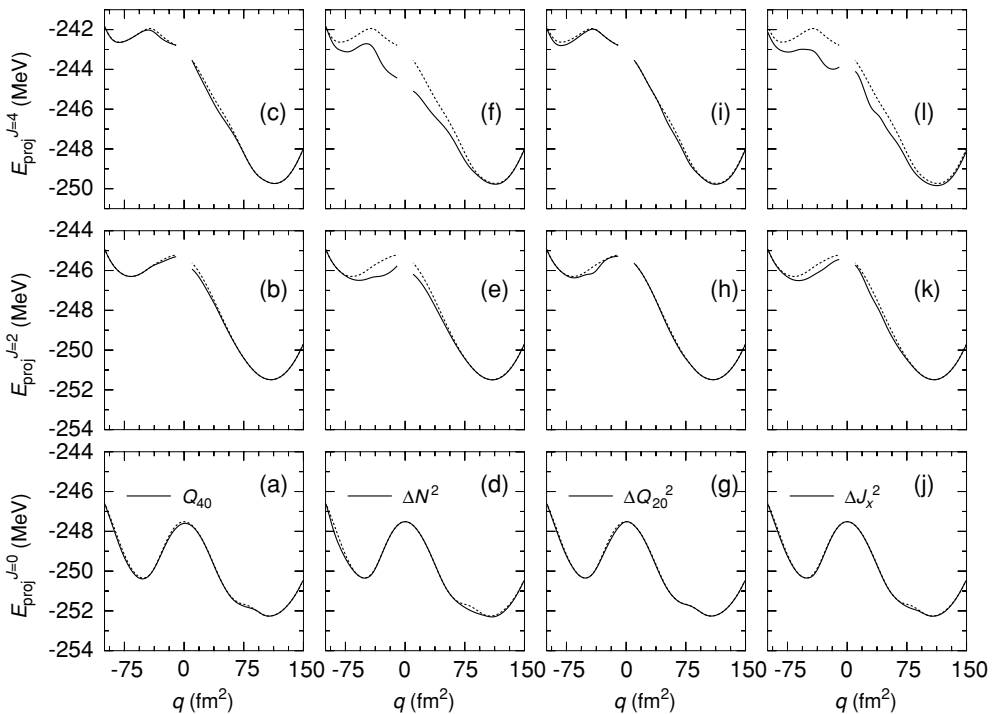
FIG. 5. Same as Fig. 4 but for the nucleus ^{34}Mg.

TABLE II. The GCM energies for the lowest lying states with angular momenta $J = 0$, 2, and 4, as well some energy differences. Each column corresponds to a different set of generating functions and "single" in this context means that only the constraint on the quadrupole moment q is considered. The quantity $\Delta E^{J=0}$ is the energy difference between the GCM calculation that includes the effect of the additional constraint and the one that does not include it. See text for further details.

	Constraint				
	Single	Q_{40}	ΔN^2	ΔQ_{20}^2	ΔJ_x^2
$E^{J=0}$ (MeV)	-246.744	-246.753	-246.837	-246.751	-246.794
$E^{J=2}$ (MeV)	-245.271	-245.274	-245.285	-245.281	-245.285
$E^{J=4}$ (MeV)	-243.172	-243.173	-243.247	-243.273	-243.297
$\Delta E^{J=0}$ (keV)	0.0	9	93	7	50
$E_{2^+} = E^{J=2} - E^{J=0}$ (MeV)	1.473	1.479	1.562	1.470	1.509
$E_{4^+} = E^{J=4} - E^{J=0}$ (MeV)	3.572	3.580	3.590	3.478	3.497

additional degrees of freedom with $\Delta K \neq 0$ are needed (i.e., the kind of triaxial and time reversal breaking configurations mentioned in Sec. I and not taken into account in the present work), as they will push down the $J = 2$ energy but leave the $J = 0$ energy unaffected. Obviously, the additional degrees of freedom considered in this paper are of the $\Delta K = 0$ kind, and therefore they cannot induce the mentioned effects. The $E^{J=4}$ energies change in amounts similar to those in the $J = 2$ case, the change being bigger for the $\langle \Delta \hat{N}^2 \rangle$, $\langle \Delta \hat{Q}_{20}^2 \rangle$, and $\langle \Delta \hat{J}_x^2 \rangle$ additional constraints. This is again consistent with the tiny change observed in 4 around the $J = 4$ absolute minimum. The E_{4^+} energies change by tiny amounts, with the $\langle \Delta \hat{Q}_{20}^2 \rangle$ constraint being the most significant with a reduction of the E_{4^+} energy of only 94 keV. At this point, let us mention that the results obtained for the GCM calculation for the nucleus ^{32}Mg could have been anticipated by looking at Fig. 4 and observing that the additional constraints did not change the AMP energy landscape around the absolute minima. As a consequence, and because of the corresponding plots for ^{34}Mg (see Fig. 5), we have decided not to carry out a similar GCM calculation for this nucleus as the results would be similar to those already discussed for ^{32}Mg. Finally, as a general conclusion, we can say that the GCM results corresponding to the lowest lying states remain almost unaffected by the inclusion of the additional constraints considered in this paper. On the other hand, among the extra degrees of freedom considered, the $\langle \Delta \hat{N}^2 \rangle$ and $\langle \Delta \hat{J}_x^2 \rangle$ ones might play a quantitative role for higher lying states and angular momenta greater than 0.

IV. CONCLUSIONS

With the aim of testing the stability of previous results obtained for the nuclei ^{32}Mg and ^{34}Mg, which were obtained in the framework of a restricted variation after angular momentum projection where the quadrupole moment was the parameter chosen to parametrize the reduced variational Hilbert space, we have enlarged the variational Hilbert space for the projected energies by the inclusion of additional wave functions obtained by constraining the mean values $\langle \hat{Q}_{40} \rangle$, $\langle \Delta \hat{N}^2 \rangle$, $\langle \Delta \hat{Q}_{20}^2 \rangle$, and $\langle \Delta \hat{J}_x^2 \rangle$ corresponding to axially symmetric operators. The projected energy landscapes obtained, as well as the results of additional GCM calculations, indicate that the extra degrees of freedom considered only induce minute changes on the energies of the lowest lying state for each angular momentum $J = 0$, 2, and 4. We therefore conclude that, in order to include correlations to describe the lowest lying states in the present framework, the relevant axially symmetric degree of freedom to be considered is the one associated with the quadrupole moment operator. Obviously, the present results do not rule out the relevant role triaxiality and/or time reversal breaking might have for $J \neq 0$ states.

[1] M. Bender, P. H. Heenen, and P.-G. Reinhard, Rev. Mod. Phys. **75**, 121 (2003).

[2] J. L. Egido, L. M. Robledo, and R. Rodríguez-Guzmán, Phys. Rev. Lett. **93**, 082502 (2004).

[3] P.-G. Reinhard, D. J. Dean, W. Nazarewicz, J. Dobaczewski, J. A. Maruhn, and M. R. Strayer, Phys. Rev. C **60**, 014316 (1999).

[4] T. R. Werner, J. A. Sheikh, M. Misu, W. Nazarewicz, J. Rikovska, K. Heeger, A. S. Umar, and M. R. Strayer, Nucl. Phys. **A597**, 327 (1996).

[5] G. A. Lalazissis, D. Vretenar, P. Ring, M. Stoitsov, and L. M. Robledo, Phys. Rev. C **60**, 014310 (1999).

[6] J. F. Berger, J. P. Delaroche, M. Girod, S. Péru, J. Libert, and I. Deloncle, Inst. Phys. Conf. Ser. **132**, 487 (1993).

[7] A. Valor, P.-H. Heenen, and P. Bonche, Nucl. Phys. **A671**, 145 (2000).

[8] R. Rodríguez-Guzmán, J. L. Egido, and L. M. Robledo, Phys. Lett. **B474**, 15 (2000); Phys. Rev. C **62**, 054319 (2000).

[9] C. Détraz, D. Guillemaud, G. Huber, R. Klapisch, M. Langevin, F. Naulin, C. Thibault, L. C. Carraz, and F. Touchard, Phys. Rev. C **19**, 164 (1979).

[10] D. Guillemaud-Mueller, C. Détraz, M. Langevin, F. Naulin, M. De Saint-Simon, C. Thibault, F. Touchard, and M. Epherre, Nucl. Phys. **A426**, 37 (1984).

[11] T. Motobayashi *et al.*, Phys. Lett. **B346**, 9 (1995).

[12] B. V. Pritychenko *et al.*, Phys. Lett. **B461**, 322 (1999).

[13] V. Chisté *et al.*, Phys. Lett. **B514**, 233 (2001).

[14] H. Iwasaki *et al.*, Phys. Lett. **B522**, 227 (2001).

[15] P. Ring and P. Schuck, *The Nuclear Many Body Problem* (Springer-Verlag, Berlin, 1980).

[16] K. Hara and Y. Sun, Int. J. Mod. Phys. E **4**, 637 (1995).

[17] J. L. Egido and L. M. Robledo, Lect. Notes Phys. **641**, 269 (2004).

[18] R. Rodríguez-Guzmán, J. L. Egido, and L. M. Robledo, Nucl. Phys. **A709**, 201 (2002).

[19] K. W. Schmid and F. Grümer, Rep. Prog. Phys. **50**, 731 (1987); K. W. Schmid, Prog. Part. Nucl. Phys. **52**, 565 (2004).

[20] J. Decharge and D. Gogny, Phys. Rev. C **21**, 1568 (1980).

[21] J. F. Berger, M. Girod, and D. Gogny, Nucl. Phys. **A428**, 23c (1984).

[22] T. R. Rodríguez, J. L. Egido, L. M. Robledo, and R. Rodríguez-Guzmán, Int. J. Mod. Phys. E **13**, 165 (2004).

[23] J. L. Egido, J. Lessing, V. Martin, and L. M. Robledo, Nucl. Phys. **A594**, 70 (1995).